ELSEVIER

Ceramics International 25 (1999) 183–190

CERAMICS INTERNATIONAL

Reduction in specific surface area of an alumina powder at a relatively low temperature

Takayasu Ikegami *, Yoshizou Kitami, Masayuki Tsutsumi

National Institute for Research in Inorganic Materials, 1-1, Namiki, Tsukuba-shi, Ibaraki, Japan

Received 10 September 1997; accepted 15 December 1997

Abstract

A highly sinterable $A1_2O_3$ powder and its powder compact are simultaneously fired up to a given temperature at a constant rate of heating. The specific surface areas, S_p, of them decrease appreciably from 700°C, but there is a slight difference in the S_p value between them in the low temperature region from 700 to 950°C. This similarity suggests both slight neck growth and reduction of the S_p values through not only smoothing of rough surfaces but also disappearance of peculiarly small particles. Above 950°C, on the other hand, appreciable neck growth results in more rapid decrease of the S_p value for the powder compact than for the powder. These explanations are well consistent with other empirical data, both variations of shrinkage curves and the particle size distributions by preliminary firing.

Keywords: A. Sintering; C. Diffusion; D. Al_2O_3; Surface area reduction

1. Introduction

Classical sintering theories [1–8] have produced the five sintering mechanisms, surface diffusion [2,4], evaporation–condensation [2–4], grain-boundary diffusion [5,6] volume diffusion [2–6], and flow [1,3]. The surface diffusion mechanism and the evaporation–condensation mechanism in them cause only neck growth between particles. The other mechanisms, on the other hand, bring about not only neck growth but also shrinkage between particles. Densification of a powder compact, thus, occurs in the case where the latter mechanisms operate.

Ashby [9] summarized the accumulated information on sintering of metals in his sintering diagrams. According to these diagrams, the surface diffusion mechanism is predominant in a relatively lower temperature region in comparison with not only the volume diffusion mechanism but also the grain-boundary diffusion mechanism. This relation must also be probable for sintering of ceramics. Gray [10], for example, reported that the rate controlling step of zinc oxide changes from diffusion in surface zone in the low temperature region to such steps as lattice or complex diffusion and viscous-flow mechanism about the Tammann temperature. Prochazka and Coble [11], also explained appreciable decrease of surface area of alumina above 700 to 800°C with the surface diffusion mechanism. This explanation consists with reported data that considerable densification of alumina [12–14] has occurred usually above 1000°C. German and Munir [15] dealt with sintering by the surface diffusion mechanism in both the cases of ceramics and powder metallurgy in detail. Recent densification data [16] for a sinterable $A1_2O_3$ powder, however, suggested negligible neck growth prior to beginning of shrinkage. The present study traced an origin for these controversial data.

2. Kinetic equations for reduction in surface area

Notation ΔS designates a specific surface area reduction in per cent from the starting one, S_o. That is, S_o equals the sum of S_p and the product of ΔS and S_o where S_p is a specific surface area of a fired sample. A differential kinetic equation [15] in respect to ΔS is given as

$$\Delta S^{m-1} \mathrm{d}\Delta S = K_O \exp\left(\frac{E}{RT}\right) \mathrm{d}t \quad (1)$$

* Corresponding author.

0272-8842/99/$—see front matter
PII: S0272-8842(98)00022-4

in general, where m is a constant characterized by the model of surface area reduction, E is an activation energy for the mass transfer, RT has the usual meaning and t is a firing time. When a single mechanism is predominant, not only m and E but also factor K_o are constants. If plural mechanisms of mass transfer concurrently contribute to surface area reduction, the values of them change during the reduction process concerned. If this is the case, the calculation of Eq. (1) is very difficult. Then, to simplify the problem, a single mechanism is assumed in the present study (assumption (1)). The variables, ΔS and t, in Eq. (1) are separated into its left-hand side and right-hand side, respectively. This separation allows the independent integration of each side. Integrating the left-hand side of Eq. (1) results in

$$\int_{s_i}^{s_j} \Delta S^{m-1} \mathrm{d}\Delta S = (\Delta S_j^m - \Delta S_i^m)/m \tag{2}$$

where ΔS_i and ΔS_j are the gross values of reduction in S_p at the initial time, t_i, and the final time, t_j, respectively. In a usual reducing model of surface area, ΔS_i equals zero at the beginning geometry defined by the model concerned. If the powder or the powder compact has already a geometry on the way of the surface reduction process before firing, ΔS_i has a considerable value. Thus, ΔS_j equals the sum of ΔS_i and ΔS or $\Delta S_j = \Delta S_i + \Delta S$,where ΔS is an apparent decrease of S_p during firing.

If m is an integer, Taylor's expansion [17] of function $F(\Delta S_j) = (\Delta S_i + \Delta S)^m$ results in $F(\Delta S_j) = F(\Delta S_i) + F'(\Delta S_i)\ \Delta S/1! + F''(\Delta S_i)\ \Delta S^2/2! -$, and then

$$\Delta S_j^m - \Delta S_i^m = m\Delta S_i^{m-1}\Delta S + \frac{m(m-1)}{2}\Delta S_i^{m-2}\Delta S^2 + m\Delta S_i \Delta S^{m-1} + \Delta S^m \tag{3}$$

An empirical study has usually ignored the second term, ΔS_i^m, in the left hand side of Eq. (3), and used the term of $\Delta S^{m'}$ instead of $\Delta S_j^m - \Delta S_i^m$, where m' is an apparent exponent neglecting the effect of the ΔS_i value. If $\Delta S_i << \Delta S$ ($\Delta S_j \fallingdotseq \Delta S$), this neglect is practically valid, and the m' value can approximate to the m value.

If ΔS_i has a considerable value against the aforesaid assumption, the condition of $\Delta S << \Delta S_i$ is surely satisfied at the beginning of a firing process. For such a case, $\Delta S/\Delta S_i >> (\Delta S/\Delta S_i)^2 >> \text{--} >> (\Delta S/\Delta S_i)^m$. The right-hand side of Eq. (3), thus, can approximate to the first term, $m\Delta S_i^{m-1}\Delta S$; and then the m' value nearly equals unity. The ΔS value increases during firing, approaching initially to the ΔS_i value. After the former gets the latter, the relation between them is turned and $\Delta S_i < \Delta S$. Further firing must result in the relation, $\Delta S_i << \Delta S$, finally. According to Eq. (3), the variation of the relation concerned means change of the m' value from 1 to m during firing.

For isothermal heating, the right-hand side of Eq. (1) has only the variable, t. Integration of this side results in

$$\int_{t_i}^{t_j} K_o \exp(-\frac{E}{RT})\mathrm{d}t = K_o \exp(-\frac{E}{RT})(t_j - t_i) \tag{4}$$

For a constant rate of heating (CRH), T is directly proportional to t and $T = H_c t$, where H_c is a heating rate. Though the relation between T and t is simple, the algebraic integration of $\exp(-E/RT)$ is impossible. Woolfry and Bannister [18], then, estimated the integration concerned as

$$K_o \int_{t_i}^{t_j} \exp(-\frac{E}{RT})\mathrm{d}t = \frac{K_o R}{H_c E}[T_j^2 \exp(\frac{E}{RT_j}) - T_i^2 \exp(\frac{E}{RT_i})] \tag{5}$$

where T_i is the starting temperature and T_j is the highest temperature, respectively. The integration of Eq. (5) is valid only in the case where both the values of K_o and E are constants. A predominant mechanism, then, must keep in the temperature range between T_i and T_j. Since the value of $\exp(-E/RT)$ abruptly increases with elevating the firing temperature, the $T_j^2 \exp(-E/RT_j)$ value is enormously larger than the $T_i^2\exp(-E/RT_i,)$ value in general. When the value of $T_i^2\exp(-E/RT_i)$ is neglected, combining Eqs. (3) and (5) results in

$$\Delta S_j^{m\prime} = \frac{K_o R}{H_c E} T_j^2 \exp(-\frac{E}{RT_j}) \tag{6}$$

The term of $T_j^2\exp(-E/RT_j)$ has a unique value for a given temperature irrespective of a heating rate, H_c. If the S_p value at a temperature, T_1, for the heating rate of H_1 equals that at a temperature, T_2, for the heating rate of H_2, the equation, $T_1^2\exp(-E/RT_1)/H_1, = T_2^2\exp(-E/RT_2)\ /H_2$, is derived from Eq. (6). After general logarithms are taken for both the sides of this equation, factor E and the rest factors are separated into both the sides of an equation as

$$E = R\ln(H_2 T_1^2/H_1 T_2^2)/(1/T_1 - 1/T_2) \tag{7}$$

This equation evaluates the activation energy, E. Eq. (6), on the other hand, is rearranged in respect to both the factor of T_j and the rest factors as $T_j^2\exp(-E/RT_j) = \Delta S_j^{m'} H_c E/K_o R$. This equation produces equality $\Delta S_1^{m'} H_1 = \Delta S_2^{m'} H_2$ in the case where firing temperatures

are equal between the two different heating schedules of H_1 and H_2. The m' value is evaluated from this equality as

$$m' = \log(H_2/H_1)/\log(\Delta S_1/\Delta S_2) \quad (8)$$

where ΔS_1 and ΔS_2 are ΔS for the heating rates of H_1 and H_2, respectively.

3. Experimental

3.1. Sample Preparation

A purchased alumina powder (AKP-20, Sumitomo Chem. Co. Ltd., Osaka, Japan and major impurities of Si = 15, Na = 3, Ma = 3, Cu < 1 and Fe = 8 in ppm by weight) was dispersed in ethyl alcohol for 20 min with an ultrasonic agitator. The resulting dispersion was stirred at about 70°C by a magnetic stirrer with a heat element to evaporate the ethyl alcohol. The dried powder was calcined at 500°C for 2 h, lightly crushed with an alumina mortar and an alumina pestle, and then sieved on weighting sheets to collect particles with size less than 170 mesh. The resulting powder was divided into four parts to make four kinds of samples, A to D.

A: The first part of the divided powders was pressed in 12-mm die at 20 MPa, and hydrostatically pressed at 200 MPa. The dimensions of the powder compacts were 11 mm in diameter and 5 mm long. One of these powder compacts was put into a high alumina boat, set in a furnace, and fired up to a given temperature at a heating rate of 1.1, 3.3, 10 or 60°C min in flowing O_2 gas. Just after getting a given temperature, the sample was cooled down at the same rate as the rising.

B: In both the cases of the heating rates of 1.1 and 60 °C min^{-1}, a small amount, about 1 g, of the sieved powder was put by the aforesaid powder compact in the alumina boat, and fired along with it.

The notation of a type, PQR, represents not only the type of the samples, A and B, but also the firing conditions. The first letter, P, of this notation designates the type of the samples, and thus letter P is replaced by A for type A or B for type B in the actual notation.

Letter Q in PQR is the numeral designating a heating rate, and the used numeral is 1 for 1.1°C min^{-1}, 2 for 3.3 °C min^{-1}, 3 for 10°C min^{-1} and 4 for 60°C min^{-1}. Letter R in PQR is replaced by the numeral designating the maximum temperature; the used numeral is 1 for 700°C, 2 for 780°C, 3 for 820°C, 4 for 860°C, 5 for 910°C, 6 for 960°C, 7 for 1000°C, and 8 for 1100°C. Notation B24, for example, indicates that the sample is type B, the heating rate is 3.3°C min^{-1}, and the maximum temperature is 860°C.

C: With the third part, powder compacts were made by the same method as sample A was done. One of the resulting powder compacts was fired isothermally at 800, 900 or 1000°C for 2 h in flowing O_2 gas. The dimensions of both the green and the fired powder compacts were measured with a micrometer. Samples A to C were mainly used for measurement of the S_p value.

D: With the last part, powder compacts were made in 6-mm die and hydrostatically pressed. The pressures for both pelletting and hydrostatic pressing equalled those for sample A, respectively. The resulting dimensions of the powder compacts were 5.5 mm in diameter and 5 mm long. One of the powder compacts was pre-fired by the same conditions as sample C was done, and then examined its sintering behaviour.

Letter S of notation type, S_T, is replaced, respectively, by letter C or D to designate sample C or D; subscript T indicates a pre-firing temperature. Notation C_{800}, for example, indicates that the type of a sample is C and the pre-firing temperature is 800°C. The green compact of type D was exceptionally designated as D_{25}.

3.2. Observation of the particle shapes by scanning electron microscopy (SEM) and transmission electron microscopy (TEM)

The shapes of particles were observed by SEM (S-5000, Hitachi Co., Tokyo) and by TEM (JEM-2000EX, JEOL Co., Tokyo).

3.3. S_p measurement

The sample of type A or C was broken on a steel block with a steel rod and sieved to collect particles having radii 170 to 1000 μm.The S_p values of not only these broken particles but also powder B were measured two times by BET method with N_2 gas at −196°C using an automatic surface area analyser (Model 4201, Beta Scientific Co., Long Island, N.Y.). Difference in the S_p value between the first and the second runs was less than 1% for most samples. If the difference concerned exceeded 1%, further S_p measurement was done several times. Both the largest and the smallest S_p values were excluded from calculating the average of the measured S_p values.

3.4. Particle size distribution (PSD) measurement

To evaluate a degree of neck growth roughly, the samples of both type A, the powder, and type B, the powder compact, were crushed with an alumina mortar and an alumina pestle for 10 min, respectively. After the crushed pieces were dispersed ultrasonically in 0.1 wt% sodium hexametaphosphate aqueous solution for 10 min, their PSD was measured by laser diffraction and scattering method (Type 1064, Cilas, Marcoussis, France).

3.5. Sintering during a constant rate of heating (CRH)

The powder compact of type D was fired at the heating rate of 3.3°C min^{-1} up to 1500°C, and the shrinkage of it was measured with a thermomechanical analyser, TMA (TMA-1700, Rigaku Co., Tokyo). After measured the shrinkage, the dimensions of the fired compact were measured with a micrometer.

4. Results

The green density, ρ_S, of types A, C and D was 59.2% of theoretical. TEM micrographs in Fig. 1 show both (A) a smooth surface and (B) a rough surface of the sieved particles. The frequency of the rough surfaces was not so smaller than that of the smooth ones. Fig. 2 shows the SEM micrographs of (A) the sieved powder, (B) A14, (C) B14 and (D) A18. The sieved powder in Fig. 2(A) had (a) very small flakes as well as (b) particles with rough faces. Rising a firing temperature resulted in not only disappearance of the small flakes but also smoothing the particle surfaces. The arrows in Fig. 2(D) also show the relics of grown necks between particles.

The S_p value of the sieved powder equated 5.46 $M^2 g^{-1}$. Pelletting and/or firing at 500°C for 2 h induced slight reduction of surface area to 5.35 $M^2 g^{-1}$. The

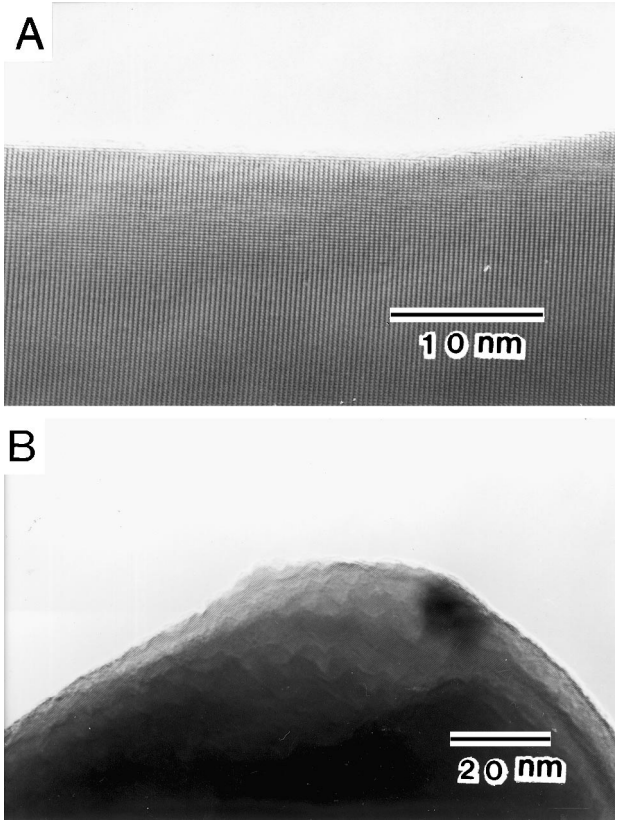

Fig. 1. TEM micrographs: (A) flat surface and (B) rough surface.

latter value was used as the starting specific surface area, S_o. Fig. 3 shows the relation between the ΔS value of sample A vs a firing temperature for the four heating rates. The relations concerned were characterized by the two regions, namely the lower temperature region between 700 and 820°C, and the higher temperature region from 820°C. The values of m' and E were 4.1 and 970 kJ mol^{-1} for the former region, and 7.2 and 550 kJ mol^{-1} for the latter region, respectively. Fig. 4 shows the S_p values of both samples A and B as a function of firing temperature. There was a small difference in the S_p value between samples A and B up to 950°C at both the heating rates of 1.1 and 60°C min^{-1}. Above 950°C, the powder compact, type A, had a smaller S_p value than the powder, type B. The difference in the S_p value between types A and B became large with rising temperature, especially for the slow heating rate of 1.1°C min^{-1}.

Pre-firing for 2 h reduced noticeably the S_p value of type C by 11% of S_o for pre-fired temperature of 800°C, by 16% for 900°C, and by 23% for 1000°C. The same firing conditions, on the other hand, resulted in a slight shrinkage of type D by 0.05% for 800°C, by 0.06% for 900°C and by 0.96% for 1000°C. Similar shrinkages were measured between the diameter and the height of the pre-fired compact. The CRH shrinkage curves in Fig. 5 show that the pre-firing at a relatively low temperature like 800°C and 900°C reduced an apparent shrinkage, ΔL ($=\Delta L_j - \Delta L_i$), only in the low temperature region up to 1150°C. Such reduction, however, extended to the whole temperature region for D_{1000}. After the CRH measurement, a similar shrinkage was detected between the diameter and the height of a sintered compact irrespective of prefiring temperature.

Fig. 6 shows that the volume of particles with radii larger than 2 μm was negligibly small in the sieved powder, of which the PSD was close to that of B14. The PSDs of A14 and B18 had small amounts (2 to 3 vol%) of relatively large particles in the range between radii 10 to 20 μm. The PSD of A18, on the other hand, showed trimodal distributions from 0.1∼2 μm, 2∼30 μm and 30∼70 μm.

5. Discussion

Calcining a mother salt usually resulted in agglomerates of primary particles in which necks had grown appreciably. If this is the case, and if only neck growth causes reduction of S_p, Eq. (3) indicates that the m' value nearly equals unity in the lower ΔS region. Fig. 3, however, indicates the apparently large m' value ($=4$) even from $\Delta S = 0.1\%$. This evaluation suggests three possibilities: the first of them was that necks grew negligibly among particles in the starting powder. The neck growth resulted in reducing the S_p value. The second

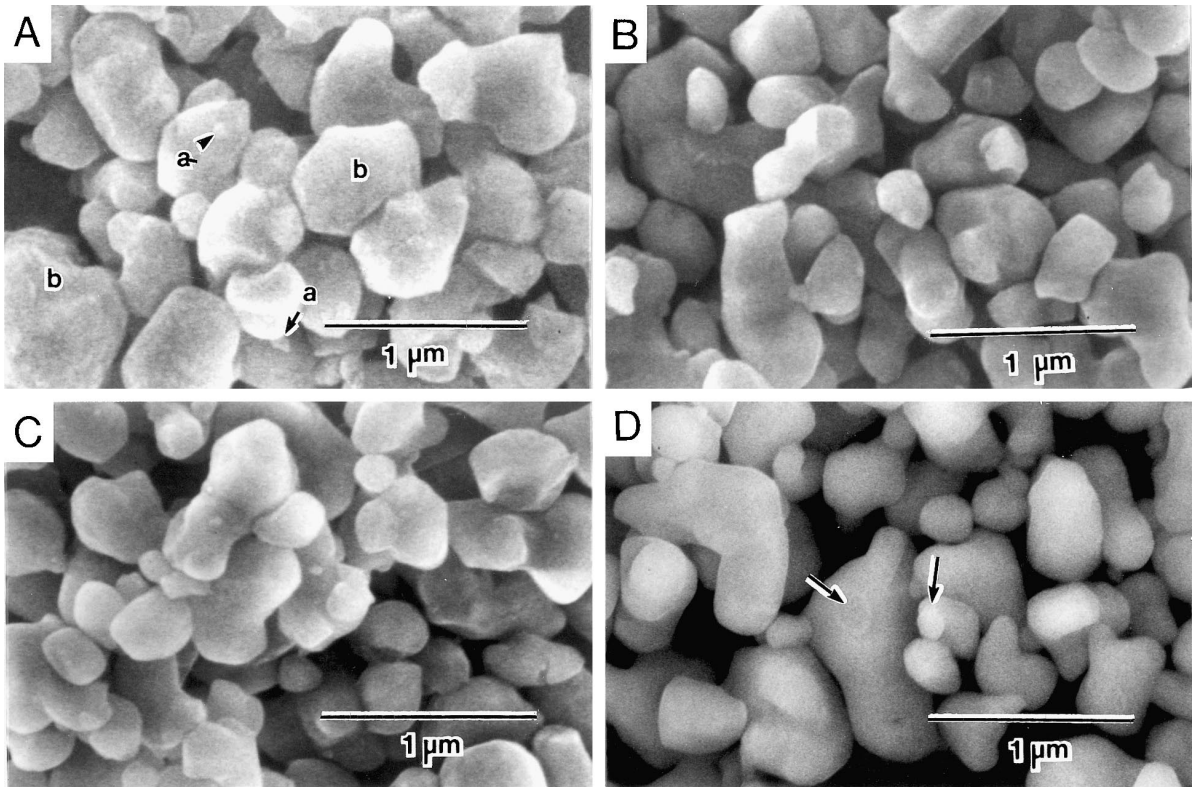

Fig. 2. SEM micrographs: (A) sieved powder which had small flakes, a, and particles with rough surfaces, b, (B) A14, (C) B14 and (D) A18. A18 had grown necks indicated by arrows.

possibility is opposite to the first case, that is, necks had grown in agglomerates. The decrease of the S_p value, then, was caused predominantly by neck growth between particles on the neighboring circumferences of the agglomerates. Such necks, however, were very few in the necks of the powder compact, and thus explaining hardly the appreciable decrease of the S_p value, 20% of S_o, from 700 to 950°C in Fig. 4. The last possibility is the reduction of S_p without neck growth between particles, that is, smoothing the rough surfaces of particles or selected disappearance of peculiarly small particles.

Reported simulation experiments [19,20] have evaluated a coordination number, n_c among particles in a loose powder as 2 to 4. A powder compact with $\rho = 59\%$, on the other hand, has the n_c, value [21] of 7 to 9. If neck growth causes reduction of the S_p value, increase of the n_c value causes more rapid decrease of the S_p value for the powder compact than for the powder.This evaluation well explained the experimental S_p values from 950°C in Fig. 4, in which the S_p value decreased more quickly for the powder compact than for the powder. Furthermore, the relics of neck growth were observed in the microstructure of A18. Slight neck growth, on the other hand, was indicated in the lower temperature region from 700 to 950°C because of the close S_p values between the powder compact and the powder, ruling out the first possibility. It was already

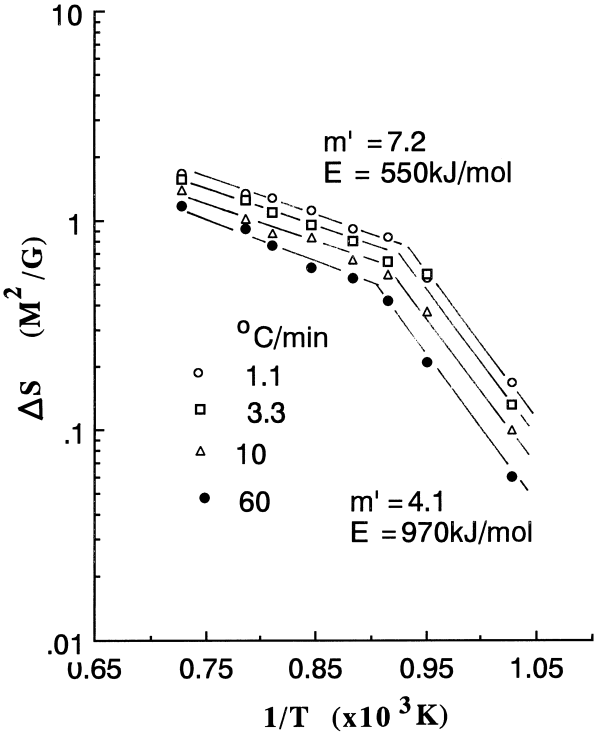

Fig. 3. Reducing the specific surface area as a function of firing temperature for four heating rates. The dots are the ΔS values of PQR (P: A, Q: 1 to 4 and R: 1 to 8). The m' value approximated to the m value because of its value appreciably larger than unity.

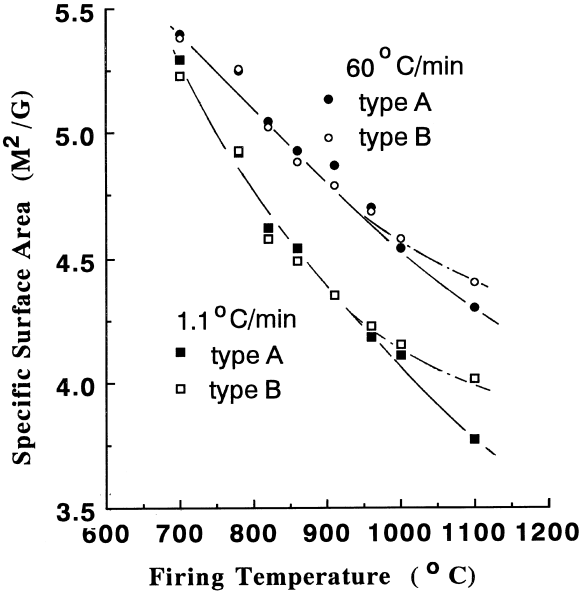

Fig. 4. Relation between S_p and firing temperature for samples A (powder compact) and sample B (powder). The dots are the S_p value of PQR (P: A and B, Q: 1 or 4 and R: 1 to 8).

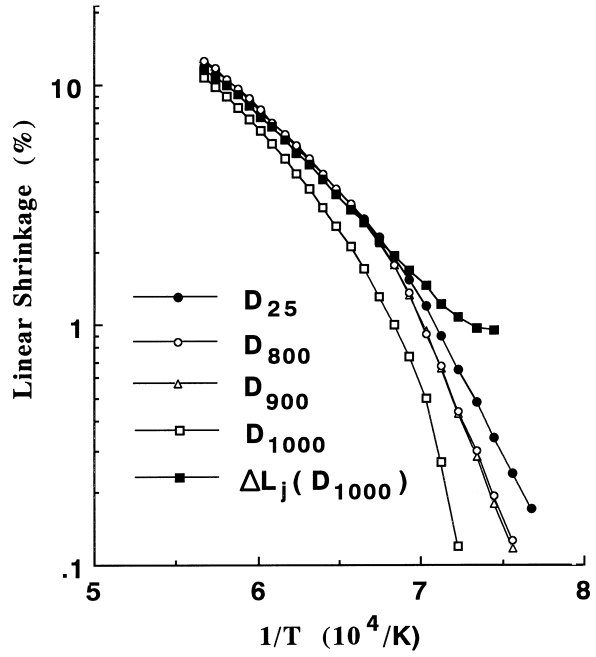

Fig. 5. Relation between apparent shrinkage, ΔL, and temperature. The gross shrinkages, ΔL_j, of D_{800} and D_{900} were described with the ΔL value of D_{25} from $\Delta L = 0.1\%$. The ΔL_j value of D_{1000}, on the other hand, was nearly constant below 1100°C.

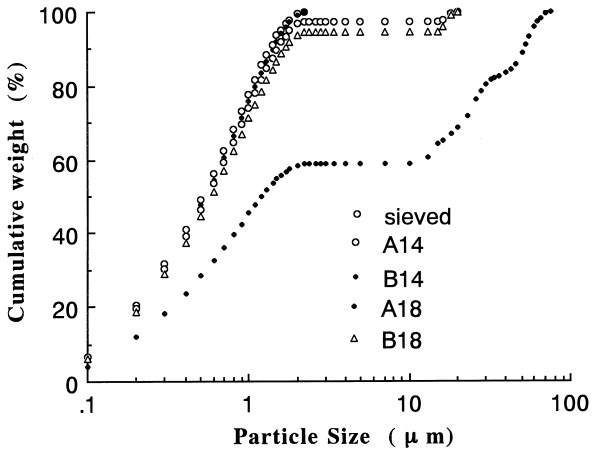

Fig. 6. Variation of particle size distributions (PSD) by preliminary firing.

verified that the second possibility was small; and then the third possibility was most plausible for the present experiment.This conclusion is supported by the microstructures (A) to (D) in Fig. 2. As can be seen there, during firing from 700 to 1100°C, not only small flakes disappeared, but also the rough surfaces became smooth.

The present powder was ball-milled on the half way of the fabrication process in its supplier. It seems reasonable that the ball-milling induced complicated stresses on the powder, generating not only small flakes but also rough particle surfaces. Such stresses were so complicated that difficult description must be done for the geometry of the rough surfaces concerned, which was drawn tentatively with simple hemispherical hillocks and valleys of radius r_s. The surface area of the hillocks and valleys equals $2\pi r_s^2$. The base area of them, on the other hand, equals πr_s^2. The ratio of the former area to the latter area equals 2 irrespective of size of the hillocks and valleys concerned. This constant value indicates that even if the hillocks and valleys are negligibly smaller in size than the particles, the S_p value of particles with the rough surfaces decreases to half of the initial one through smoothing the roughness.

The distance of diffusion, x, can be estimated roughly as $x = k_d\sqrt{Dt}$ where D is the self-diffusion coefficient, and k_d is a constant. While a neck radius increases to x, the rough surfaces become smooth by the mass transfer between the hillocks and the valleys with radius $x/2$. If x equals one tenth of the particle size — if the volume diffusion and/or the grain-boundary diffusion mechanism is predominant, this neck growth causes a negligible shrinkage of $\Delta L = 0.25\%$ — the surface area of a particle decreases by about 0.2% per neck for the sphere–sphere models [2–4], and about 0.3% for the line contact model [22]. The n_c value was estimated as 7 to 12 for a powder compact. The neck growth in a powder compact, then, reduces the S_p value by 1.5 to 2.4% of S_o. for the usual models and 2.1 to 3.6% for the line contact model. If the x value is less than one tenth of the particle size, reducing the S_p value by neck growth is more slight than the foregoing estimation. This relation is in contrast with the constant reduction of about 50% by smoothing rough surfaces. Fig. 1(B) shows that the hillocks and valleys concerned are less in size than one twentieth of the particle. It was no wonder that since the

hillocks and valleys concerned were very small, smoothing of the rough surfaces occurred along with negligible shrinkage at a lower temperature like 700°C.

An activation energy is usually smaller in the lower temperature region than in the higher temperature one, in contrast with the data in Fig. 3. It was difficult to verify an origin for the present unusual data because of limited knowledge on the conditions of the surfaces.

The PSD of A14 in Fig. 6 was similar to that of the sieved powder except a small amount (2 to 3 vol%) of particles with radii from 10 to 20 μm. This similarity suggests that contacts or necks among primary particles were so weak that most of them were collapsed ultrasonically. Relatively large particles from 2 to 70 μm in the PSD of A18 were considerably more in number than those in B18. This difference in number of large particles may be attributable to that compaction of the powder increased the n_c value, and thus enhanced solidification of many primary particles which was due to neck growth by sintering. If, on the other hand, the PSD was homologized by the cumulative weight at the particle size of 2 μm, all the PSD in Fig. 6 were close each other irrespective of both the sample type and the firing temperature. This similarity suggests that the present compacting or crushing did not break major of the primary particles in the starting powder.

A densification rate, $d\Delta L/dt$ [2–6], is expressed by an equation similar to Eq. (1) as

$$\frac{d\Delta L}{dt} = \frac{K_d}{\Delta L^{n-1}} \tag{9}$$

where n is a constant dependent on the sintering mechanism, and K_d is a factor remarkably dependent on a temperature. Integrating this equation results in

$$\Delta L_j^n = \Delta L_i^n + \int_{T_i}^{T_j} K_d dT/H_c' \tag{10}$$

for CRH ($T = H_c't$), where ΔL_j and ΔL_i, are, respectively, the gross shrinkages at the highest temperature, T_j, and the initial temperature, T_i. The ΔL_i value is unknown for a usual powder compact, of which the densification data, then, have been analysed with an empirical equation, $\Delta L^{n'} = \int_{T_i}^{T_j} K_d dT/H_c'$ where n' is a constant defining the apparent sintering mechanism. Eq. (3) suggests that if the n' value is appreciably larger than unity even for a small ΔL value, the ΔL_i value is negligible and n' approximates to n. This assumption just held for sintering of the present green compact because of the large n' value [16] of about 4 even for a slight ΔL value ($\fallingdotseq 0.4\%$). The ΔL_i value of the green compact, D_{25}, was negligibly small accordingly. Eq. (10), then, indicates that the ΔL^n ($\fallingdotseq \Delta L_j^n$) value for D_{25}, approximated to the integrating term, $\int_{T_i}^{T_j} K_d dT/H_c'$. To simplify the question, $n=4$ is assumed. The ratio, $\Delta L_j^4/\Delta L_i^4$, abruptly increases with slight increase of the ratio, $\Delta L_j/\Delta L_i$; the $\Delta L_j/^4\Delta L_i^4$ valueequals 2.0, 3.8, 6.55, 10.5 and 16 for the ratio, $\Delta L_j/\Delta L_i$, = 1.2, 1.4, 1.6, 1.8, 2.0, respectively. This abrupt increase of $\Delta L_j^4/\Delta L_i^4$ indicates that if the $\Delta L_j/\Delta L_i$ value becomes larger than 2, the ΔL_j^4 value is markedly larger than the ΔL_i^4 value. The ΔL_i^4 value equalled 0.05% for D_{800}, 0.06% for D_{900}, and 0.96% for $D_{1000}$and then the ΔL_j^4 value approximated to the integrating term $\int_{T_i}^{T_j} K_d dT/H_c'$ofEq. (10) from $\Delta L_j > 0.1\%$ for both D_{800} and D_{900} and from $\Delta L_j > 2\%$ for D_{1000}. These evaluations are supported with the data in Fig. 5, which shows that the ΔL value of D_{25} well fit the ΔL_j value ($=\Delta L+\Delta L_i$) not only above $\Delta L=0.1\%$ for both D_{800} and D_{900} but also above $\Delta L = 2\%$ for D_{1000} (the dashed line). The ΔL_i^4 value of D_{1000} was markedly larger than the integrating term $\int_{T_i}^{T_j} K_d dT/H_c'$ in the lower temperature region below 1110°C, and ΔL_j nearly equated ΔL_i. This equality resulted in the nearly constant value of the dashed line in the aforesaid low temperature region of Fig. 5.

Neck growth causes three phenomena: (1) reducing the driving force for sintering, (2) increase of lengths between the diffusion sources and diffusion sinks and (3) decreasing shrinkage due to increasing the contact area of the neck even if an amount of mass transfer per unit time is the same—the amount concerned [1–8] equals the product of a shrinkage and the contact area of the neck. Phenomena (1) and (2) decrease the amount concerned in actual neck growth in contrast with the assumption mentioned just earlier. Thus, an actual densification rate, $d\Delta L/dt$, decreases abruptly with increasing the ΔL value, being described by Eq. (9) with an appreciably larger n value than unity.

Pre-firing at not only 800°C and but also 900°C for a long time, 2 h, induced appreciable reduction of the S_p value (sample D), but slight shrinkage (sample C). This contrast suggested a possibility that the surface diffusion mechanism and/or the evaporation–condensation mechanism contributed to the neck growth at a relatively low temperature region up to 900°C. If this possibility was valid, the appreciable neck growth reduced the densification rates of both D_{800} and D_{900}, which must be very lower than that of D_{25}, in the lower temperature region. The gross shrinkages ($\Delta L_j=\Delta L+\Delta L_i$) of D_{800} and D_{900} in Fig. 5, however, were well described with the apparent shrinkage, ΔL, of D_{25}, from $\Delta L_j = 0.1\%$.

Such data ruled out considerable neck growth of both D_{800} and D_{900} by the surface diffusion mechanism and/or the evaporation-condensation mechanism. This conclusion accorded with the other experimental data, the S_p values in Fig. 4 and PSDs in Fig. 6.

6. Summary

The specific surface areas, S_p, were measured for both the highly sinterable $A1_20_3$ powder and its powder compact fired at a relatively low temperature from 700 to 1100°C. Both shrinkage of the powder compact and the particle size distribution were, also, measured, and the following conclusions were obtained. (1) The present S_p value from 700 to 950°C decreased through both smoothing of rough surfaces and disappearance of small flakes. (2) Above 950°C, the S_p value of the powder compact decreased more quickly than that of the powder. This difference in decreasing the S_p value was explained with neck growth by the volume diffusion mechanism and/or the grain-boundary diffusion mechanism. (3) These data about the S_p value consisted well with other empirical data such as shrinkage of the powder compact and the variation of the particle size distribution by pre-firing.

7. Acknowledgment

The authors are indebted to Drs. M. Mitomo and T. Nishimura of our institute for valuable advice concerning the PSD measurement.

References

[1] J. Frenkel, Viscous flow of crystalline bodies under the action of surface tension, J. Phys. (USSR) 9 (5) (1945) 385–391.
[2] G.C. Kuczynski, Self-diffusion in sintering of metallic particles, Trans. AIME 185 (2) (1949) 169–178.
[3] C. Herring, Effect of change of scale on sintering phenomena, J. Appl. Phys. 21 (4) (1950) 301–303.
[4] W.D. Kingery, M. Berg, Study of the initial stages of sintering solids by viscous flow, evaporation–condensation, and self-diffusion, J. Appl. Phys. 26 (10) (1955) 1205–1212.
[5] R.L. Coble, Initial sintering of alumina and hematite, J. Am. Ceram. Soc. 41 (2) (1958) 55–62.
[6] D.L. Johnson, New method of obtaining volume, grain-boundary, and surface diffusion coefficients from sintering data, J. Appl. Phys. 40 (1) (1969) 192–200.
[7] B. Wong, J.A. Pask, Models for kinetics of solid state sintering, J. Am. Ceram. Soc. 62 (3–4) (1979) 138–241.
[8] R.M. German, Z.A. Munir, Identification of the initial stage sintering mechanism using aligned wires, J. Mater. Sci. 11 (1976) 71–77.
[9] M.F. Ashby, A first report on sintering diagrams, Acta Metall. 22 (3) (1974) 275–289.
[10] T.J. Gray, Sintering of zinc oxide, J. Am. Ceram. Soc. 37 (11) (1954) 534–539.
[11] S. Prochazka, R.L. Coble, Surface diffusion in the initial sintering of alumina part III, kinetic study, Physics of Sintering 2 (2) (1970) 15–34.
[12] M. Kumagai, G.L. Messing, Controlled transformation and sintering of a boemite sol–gel by α-alumina seeding, J. Am. Ceram. Soc. 68 (9) (1985) 500–505.
[13] I.B. Cutler, C. Bradshaw, C.J. Christensen , E.D. Hyatt, Sintering of alumina at temperatures of 1400°C and below, J. Am. Ceram. Soc. 40 (4) (1957) 134–139.
[14] T.S. Yeh, M.D. Sacks, Low temperature sintering of alumina oxide, J. Am. Ceram. Soc. 71 (10) (1988) 841–844.
[15] R.M. German, Z.A. Munir, Surface area reduction during isothermal sintering, J. Am. Ceram. Soc. 59 (9–10) (1976) 379–383.
[16] T. Ikegami, An apparent sintering mechanism depending on the fabrication history of a powder, J. Ceram. Soc. Jp. 96 (10) (1988) 1037–1039.
[17] C.J. Brookes, I.G. Betterley., S.M. Loxston, Mathematics and Statistics John Wiley & Sons, London, 1966, pp. 84–116.
[18] J.L. Woolfrey, M.J. Bannister, Nonisothermal techniques for studying initial-stage sintering, J. Am. Ceram. Soc. 55 (8) (1972) 390–394.
[19] M.J. Vold, The sediment volume in dilute dispersions of spherical particles, J. Phys. Chem. 64 (1960) 1616–1619.
[20] M. Nakagaki, H. Sunada, Theoretical calculation of sedimentation volume III, the case of spherical particles without drawing interaction, J. Pharmacy 83 (1) (1963) 73–78.
[21] T. Ikegami, Y. Moriyoshi, Intermediate-stage sintering of a homogeneously packed compact, J. Am. Ceram. Soc. 67 (3) (1984) 174–178.
[22] T. Ikegami, A model for initial sintering of sinterable $A1_2O_3$, J. Ceram. Soc. Jpn. Inter. Ed. 97 (1989) 754–757.